HDGF supports anti-apoptosis and pro-fibrosis in pancreatic stellate cells of pancreatic cancer

Yi-Ting Chen[1,2,3], Chien-Feng Li[4], Tso-Wen Wang[3], Tsung-Hao Chang[5], Teng-Po Hsu[6], Jhih-Ying Chi[5], Yu-Wei Hsiao[3], and Ju-Ming Wang[2,3,7,8,9] *

[1] Medical Research Department, Chi Mei Medical Center, Tainan, Taiwan.

[2]Department of Biotechnology and Bioindustry Sciences, College of Bioscience and Biotechnology, National Cheng Kung University, Tainan, Taiwan.

[3]Institute of Bioinformatics and Biosignal Transduction, College of Bioscience and Biotechnology, National Cheng Kung University, Tainan 70101, Taiwan.

[4]Department of Pathology, Chi Mei Medical Center, Tainan, Taiwan.

[5]Institute of Basic Medical Science, College of Medicine, National Cheng Kung University, Tainan, Taiwan.

[6]Department of Life Sciences, College of Bioscience and Biotechnology, National Cheng Kung University, Tainan, Taiwan.

[7]Center of Molecular inflammation Research, National Cheng Kung University, Tainan, Taiwan.

[8]Graduate Institute of Medical Sciences, College of Medicine, Taipei Medical University, Taipei, Taiwan.

[9]Graduate institute of Medical, College of Medicine, Kaohsiung Medical University,

Kaohsiung, Taiwan.

***Correspondence:** Ju-Ming Wang, Ph.D., Department of Biotechnology and Bioindustry Sciences, College of Bioscience and Biotechnology, National Cheng Kung University, Tainan, Taiwan; Phone: +886-6-2757575 ext. 31067; FAX: +886-6-2083663; E-mail: yumingw@mail.ncku.edu.tw

Running title: HDGF for anti-apoptosis and pro-fibrosis.

Key words: hematoma-derived growth factor (HDGF), pancreatic stellate cells (PSCs), anti-apoptosis, and pro-fibrosis.

Funding: This work was financially supported by the National Science Council Grant (NHRI-EX106-10422BI from the National Health Research Institute and MOST 106-2320-B-006-063-MY3 from the Ministry of Science and Technology).

ABSTRACT

Pancreatic cancer is refractory and characterized by extensively surrounding- and intra-tumor fibrotic reactions that are contributed by activated pancreatic stellate cells (PSCs). Activation of PSCs is critical for developing fibrotic reactions to affect pancreatic cancer cells (PCCs) or themselves. In our study, hepatoma-derived growth factor (HDGF) was secreted from transforming growth factor-β1 (TGF-β1)-activated PSCs. We revealed that HDGF contributed to anti-apoptosis and activation of PSCs leading to deposition of extracellular matrix proteins. TGF-β1 activated CCAAT/enhancer binding protein δ (CEBPD) through non-SMAD signaling; CEBPD-induced hypoxia inducible factor-1α (HIF-1α) consequently up-regulated HDGF. *In vivo* co-implantation of PCCs and HDGF knockdown PSCs exhibited a diminished fibrotic reaction. Pancreatic cancer specimens showed that severe stromal growth positively correlated with stromal HDGF and CEBPD. Our results suggest that TGF-β1 activates the CEBPD/HIF-1α/HDGF axis, contributing to the anti-apoptosis and pro-fibrotic reactions of PSCs. Either HDGF or CEBPD serves as potent therapeutic targets for disrupting fibrotic reactions.

INTRODUCTION

Pancreatic cancer shows late detection, aggressive growth, early metastasis, resistance to chemotherapeutic drugs and radiotherapy, and strong fibrotic reactions (Habisch, Zhou et al., 2010). Strong fibrotic reactions are also reported, leading to a fibrotic hypo-vascular barrier that surrounds pancreatic tumors, resulting in poor blood perfusion in transplanted tumors in contrast to the normal pancreas (Olive, Jacobetz et al., 2009). Over the last two decades, gemcitabine has been the cornerstone of chemotherapy for all stages of pancreatic cancer and works by targeting during DNA synthesis (Binenbaum, Na'ara et al., 2015). However, compared to patients who receive the traditional chemotherapy drug fluorouracil, the median survival duration is only extended from 4.41 to 5.65 months in gemcitabine-treated patients (Burris, Moore et al., 1997). Abnormal activation of pancreatic stellate cells (PSCs) increases the outgrowth of connective tissue and secretion of extracellular matrix (ECM) proteins, leading to tissue fibrosis and impaired drug delivery to tumor tissues (Masamune, Kikuta et al., 2009, Olive et al., 2009, Wang, Li et al., 2011). Overall, pancreatic cancer is refractory to chemotherapeutic drugs due to limited drug delivery resulting from strong fibrotic reactions between the tumor mass and surrounding microenvironment (Krantz, Shields et al., 2011, Olive et al., 2009).

PSCs represent approximately 4% of all pancreatic cells (Apte, Haber et al., 1998), and these cells regulate the synthesis and degradation of ECM proteins (Apte, Pirola et al.,

2012). PSCs are a subset of pancreatic cancer-associated fibroblasts (Masamune, Watanabe et al., 2009) that provide pro-survival signals to tumors (Habisch et al., 2010, Masamune & Shimosegawa, 2009). Activation of PSCs results in enhanced proliferative rates, differentiated transformation into myo-fibroblast-like cells, and increased secretion of ECM proteins, particularly collagens (Apte et al., 2012, Masamune & Shimosegawa, 2009). As described above, activated PSCs, which are responsible for producing ECM components to develop a fibrotic microenvironment within pancreatic cancer tissues, interact with cancer cells and affect cancer cell functions, such as tumor progression, metastasis, and drug resistance (Habisch et al., 2010). Hypoxic PSCs remodel the ECM fiber architecture into an organized parallel-pattern. Pancreatic cancer cells are able to migrate throughout this re-organized architecture (Sada, Ohuchida et al., 2016). Additionally, pro-fibrotic and pro-angiogenic responses in PSCs are induced under hypoxic conditions (Masamune, Kikuta et al., 2008). The synergistic effects of fibrotic reactions and hypoxic conditions in pancreatic cancer generate a supportive microenvironment that benefits tumor progression (Erkan, Reiser-Erkan et al., 2009). Generally, the complex interplay between PSCs and pancreatic cancer cells (PCCs) leads to an overriding pro-tumorigenic effect (Moir, Mann et al., 2015).

However, recent studies have reported a surprising role of fibrosis in pancreatic cancer to restrain tumor growth through depletion or reduction of the stromal fibrotic content using

the α-smooth muscle actin-positive (α-SMA) myo-fibroblast-depleted model (Ozdemir, Pentcheva-Hoang et al., 2014) or sonic hedgehog-deficient mouse model (Rhim, Oberstein et al., 2014). These findings suggest that the PSC-generated fibrotic microenvironment is important not only for passive scaffold architecture but also as an active regulator of tumors. Hence, targeting the interaction between the tumor and stromal tissues has been suggested as a potential strategy for pancreatic tumor treatment (Kota, Hancock et al., 2017, Li, Ma et al., 2012). Increasing evidence suggests that certain secreted soluble proteins promote tumor progression while the status of PSCs switches from quiescent to active.

Transcriptional activation has been implicated in many cell features, including fibrosis. Following tumorigenesis, the cancer cell-faced environment initiates from normoxic conditions. Hypoxia inducible factor-1α (HIF-1α) is an inducible transcription factor that is generally stable under hypoxic conditions (Majmundar, Wong et al., 2010). Although the involvement and importance of HIF-1α in cancer progression in hypoxia has been fully supported, the regulation and participation of HIF-1α under normoxic conditions remain largely uninvestigated. Additionally, transcription factor CCAAT/enhancer binding protein δ (CEBPD) is induced in response to many external stimuli (Ko, Chang et al., 2015). In tumorigenesis, inactivation of CEBPD in certain cancer cells has been suggested to benefit cancer progression (Chuang, Wang et al., 2014, Ko et al., 2015, Ko, Hsu et al., 2008, Li, Tsai et al., 2015). Interestingly, activation of CEBPD in the tumor microenvironment has

been suggested to serve a pro-tumor role (Chi, Hsiao et al., 2015, Hsiao, Li et al., 2013). However, the association of CEBPD activation and regulation in stromal cells, particularly in fibroblasts, remains less investigated.

Hematoma-derived growth factor (HDGF) is detectable in the conditional medium of the human hepatoma Huh7 cell line (Nakamura, Izumoto et al., 1994) and has been suggested to play a pro-tumor role in the promotion of hepatoma cell proliferation (Enomoto, Nakamura et al., 2015, Kishima, Yamamoto et al., 2002), metastasis (Yamamoto, Tomita et al., 2006), invasion, epithelial-mesenchymal transition (Chen, Kung et al., 2012), and angiogenesis (Shih, Tien et al., 2012). The divergent HDGF functions participate in a broad range of cancer cell activities. In parallel, HDGF is correlated with hepatic fibrogenesis to serve a pro-fibrogenic role by activating the TGF-β1 pathway in hepatocytes of mice that received a bile duct ligation or carbon tetrachloride treatment (Kao, Chen et al., 2010). HDGF protein is also detectable and increased in the secretome of activated PSCs compared to quiescent PSCs (Wehr, Furth et al., 2011). However, to our knowledge, the involvement and effect of HDGF in pancreatic cancer-associated fibrosis, including its role in PSCs, and its associated contribution in cancer progression remains an open question.

In the present study, HDGF, a protein secreted from TGF-β1-activated PSCs, contributed to anti-apoptosis and the generation of the ECM protein-rich microenvironment.

We further revealed that the consequent activation of transcription factors CEBPD and HIF-1α was involved in transcriptional activation of HDGF in PSCs. CEBPD acted as a central mediator that up-regulates TGF-β1 and HDGF transcription. HDGF and CEBPD were important because they induce PSC activation and are positively associated with the severe stromal outgrowth of pancreatic cancers. In addition to providing new insights into HDGF and CEBPD biology in pancreatic cancer, these results also suggest that HDGF and CEBPD could serve as fibrotic markers for the diagnostic assistant of pancreatic cancer in Tumor/Node/Metastasis (TNM) staging as well as potent therapeutic targets for developing an inhibitor of the fibrotic reaction.

RESULTS

HDGF is responsive to TGF-β1 in PSCs, plays an anti-apoptotic role and has a pro-fibrotic effect in building the architecture of pancreatic cancer

TGF-β1 activates ECM proteins, leading to pancreatic fibrosis through activation of PSCs. TGF-β1 activate PSCs to highly express α-SMA and vimentin and rearrange F-actin, which represent markers for mesenchymal cells (Bachem, Schneider et al., 1998, Menke & Adler, 2002, Vogelmann, Ruf et al., 2001). We therefore verified these fibrogenic markers in TGF-β1-treated PSCs using RT-PCR, western blot and immunofluorescence staining. The results showed that TGF-β1 treatment induced expression of α-SMA and vimentin (**Figure 1A**). Moreover, the experimental PSCs showed a morphological change into a myo-fibroblastic shape that exhibited F-actin rearrangements (**Figure 1B**). We further verified the expression of HDGF in response to TGF-β1 in PSCs. We observed that 0.5 ng/ml of TGF-β1 has no effect on the proliferation of PSCs (**Supplementary Figure 1; (Vonlaufen, Phillips et al., 2010)**), but indeed increased the secretion of HDGF in the conditional medium of TGF-β1-activated PSCs (**Figure 1C**).

These results showed that HDGF is responsive to TGF-β1 in PSCs. However, the regulation and potential role of HDGF in PSCs and its consequent effects in pancreatic cancer remain unknown. Physically, the increased cell number results from cell

proliferation and survival. The involvement of HDGF in the proliferation of fibroblasts was previously suggested (Ooi, Mukhopadhyay et al., 2010); we therefore examined whether HDGF contributed to the anti-apoptosis of PSCs. HDGF-treated PSCs were resistant to MMS, a DNA damage inducer and activator of apoptosis (**Figure 1D**). Next, TGF-β1 treatment suppressed MMS-induced apoptosis of PSCs (**Figure 1E**), but this suppression effect was attenuated in *shHDGF* PSCs (**Figure 1F**). These results suggest that HDGF contributes to the TGF-β1-induced anti-apoptotic effect in MMS-treated PSCs. Additionally, inhibition of HDGF also attenuated expression of TGF-β1-induced fibrogenic marker genes, α-SMA, type-I collagen (COL1A2) and fibronectin (FN1) (**Figure 1G**).

Following pancreatic cancer progression, fibrosis increases in parallel with the growth of pancreatic cancer. The results described above suggest that HDGF contributes to fibroblast activation and survival. We next assessed the effect of fibroblast HDGF in the architecture of pancreatic cancer. To address this issue, PSCs and PCCs were co-cultured using a hanging drop cell culture system. The results showed that the co-culture of HDGF knockdown PSCs (*shHDGF* PSCs) and PCCs mimicked a mildly fibrotic microenvironment. mCherry-bearing *shLacZ* PSCs or *shHDGF* PSCs (mCherry/*shLacZ* PSCs or mCherry/*shHDGF* PSCs; **Supplementary Figure 2**) were individually co-cultured with EGFP-bearing PCCs (EGFP/PANC-1 or EGFP/MIA

PaCa-2 cells; **Supplementary Figure 3**). According to the z-sections of the captured images (**Supplementary Movie 1 and 2**), compared with mCherry/*shLacZ* PSCs, the constituted image showed that the sphere formation of EGFP/PANC-1 and EGFP/MIA PaCa-2 cells was smaller and separated in the mCherry/*shHDGF* PSC-orchestrated microenvironment (**Figure 1H and 1I**). These results suggest that HDGF contributes to the sphere formation of pancreatic cancer cells co-cultured with pancreatic stellate cells. These observations imply that HDGF is able to stabilize the tissue architecture of pancreatic cancer and stromal cells.

HDGF knockdown in PSCs orchestrates the fibrotic architecture, which acts as a fibrotic hypo-vascular barrier

The results suggest that HDGF is involved in generating an ECM protein-rich microenvironment resulting in stabilizing the tissue architecture of pancreatic cancer. A recent study demonstrated that dense fibrotic reactions serve as a hypo-vascular barrier (Olive et al., 2009). Therefore, the penetration of endothelial cells of blood vessels is appropriate for assessing tissue density. We performed co-implantation of PSCs and PCCs into NOD-SCID mice to determine the essentiality of HDGF in PSC-generated fibrotic reactions *in vivo*. Control *shLacZ* or *shHDGF* PSCs were individually mixed with EGFP/PANC-1 or EGFP/MIA PaCa-2 cells. To evaluate the fibrotic reactions, Picrosirius

red staining was performed to examine the abundance of collagens in tissue sections from xenografted tumors. The results showed that the abundance of collagens was reduced in xenografted tumor sections of co-implanted *shHDGF* PSCs and EGFP/PANC-1 or EGFP/MIA PaCa-2 cells (**Figure 2A and 2B**). Additionally, we performed an immunofluorescence assay to determine the distribution of subcutaneously co-implanted PSCs and EGFP/PANC-1 or EGFP/MIA PaCa-2 cells. Compared with the GFP-negative region of xenografted tumors composed of *shLacZ* PSCs, the intensity of the COL1A2 and FN1 signals was attenuated in the GFP-negative region of xenografted tumors composed of *shHDGF* PSCs (**Figure 2C to 2F**). The COL1A2 and FN1 signals was also assessed in the whole tissue sections, and the results showed that both of COL1A2 and FN1 expression was decreased in the tissue sections composed of *shHDGF* PSCs and EGFP/PANC-1 or EGFP/MIA PaCa-2 cells (**Figure 2C to 2F**). These observation was consistent with the results from Picrosirius red staining tissue sections (**Figure 2A to 2B**). Above results indicated that the loss of type I collagen and fibronectin associated with the disruption of fibrotic reactions when *shHDGF* PSCs co-cultivated with PCCs. Interestingly, expression of CD31, an associated angiogenesis and endothelial cell marker, was enhanced in the xenografted tumor sections of co-implanted *shHDGF* PSCs and EGFP/PANC-1 or EGFP/MIA PaCa-2 cells (**Figure 2G and 2H**), suggesting that the essentiality of HDGF involves in a fibrotic hypo-vascular barrier and results in attenuating

the penetration of blood vessels. This result is consistent with the suggestion that HDGF exerts a pro-fibrotic effect to orchestrate the fibrotic architecture.

TGF-β1/CEBPD/ HIF-1α axis contributes to HDGF transcriptional activation in PSCs

The results show that HDGF is responsive to TGF-β1 in PSCs. We next observed that the HIF-1α binding motif was predicted on the *HDGF* promoter via TFSEARCH (version 1.3) and PROMO (version 3.0.2), an open access website that predicts transcription factor binding sites. We first examined whether HIF-1α was responsive to TGF-β1 in PSCs. As well as HDGF expression, both *HIF-1α* mRNA and protein were up-regulated in TGF-β1-treated PSCs (**Figure 3A**). Although HIF-1α is an inducible transcript factor that tends towards stabilization under hypoxic conditions, we examined whether TGF-β1 could stabilize HIF-1α under normoxic conditions. The protein stability assay showed that TGF-β1 had no effect on HIF-1α stability (**Supplementary Figure 4**). Moreover, reporter and ChIP assays showed that HIF-1α activated the *HDGF* reporter and directly bound to the *HDGF* promoter region in response to TGF-β1 under normoxic conditions (**Figure 3B and 3C**). Considering that the cancer-stromal cell interaction should be initiated under normoxic conditions, these results imply that TGF-β1 up-regulates *HDGF* transcription during the initial stage of pancreatic tumorigenesis.

We demonstrated that TGF-β1 induced *HIF-1α* transcription in PSCs under

normoxic conditions. This result prompted us to identify the transcription factor that is involved in TGF-β1-induced *HIF-1α* transcription. Using the same strategy, the transcription factor CEBPD was predicted to bind to the *HIF-1α* promoter. To examine whether CEBPD responds to TGF-β1 and regulates *HIF-1α* transcription in PSCs, we first examined whether CEBPD is up-regulated upon TGF-β1 treatment. The results show that TGF-β1 induced *CEBPD* and auto-regulated *TGF-β1* transcripts and expression (**Figure 3D**). The reporter assay showed that exogenous expression of CEBPD activated the *HIF-1α* reporter (**Figure 3E**). Subsequently, a ChIP assay was performed to verify that CEBPD bound to the *HIF-1α* promoter under TGF-β1 stimulation. The results showed that the binding activity of CEBPD to the *HIF-1α* promoter was responsive to TGF-β1 in PSCs (**Figure 3F**).

CEBPD responds to TGF-β1 and plays an essential role in PSC activation through non-SMAD pathway-mediated reciprocal loop regulation.

The results suggest that in response to TGF-β1, CEBPD increases HIF-1α expression and consequently activates HDGF in PSCs. We further verified the upstream role of CEBPD via gain-of- and loss-of-function assays. Following exogenous expression of CEBPD in PSCs, transcription and translation of TGF-β1, α-SMA, CEBPD, HIF-1α, and HDGF were induced (**Figure 4A**). By contrast, expression of these proteins was

attenuated after CEBPD knockdown PSCs (*shCEBPD* PSCs; **Supplementary Figure 5A**) with TGF-β1 treatment (**Figure 4B**). Interestingly, in addition to up-regulation by TGF-β 1, CEBPD also reciprocally regulated TGF-β1 expression in PSCs (**Figure 4A and 4B**). Moreover, the TGF-β1-induced fibroblast-to-myofibroblast transition that accompanied F-actin rearrangement was attenuated in *shCEBPD* PSCs (**Figure 4C**).

TGF-β1 has been suggested to be a master regulator of both canonical (Smad-based) and non-canonical (non-Smad-based) signaling pathways in renal fibrosis (Meng, Nikolic-Paterson et al., 2016). To further dissect which signal pathway is involved in TGF-β1-induced CEBPD activation, the SMAD2/3 inhibitor (SB431542) was applied. The results show that SB431542 has no effect on TGF-β1-induced CEBPD activation (**Figure 4D and Supplementary Figure 6A**). We next applied various non-SMAD pathway inhibitors, including P38 inhibitor (SB203580), ERK inhibitor (U1026), and AKT/PI3K inhibitor (Wortmannin), to explore which signal pathway contributes to TGF-β1-induced CEBPD activation. The results show that CEBPD activation was significantly attenuated upon TGF-β1 combined with SB203580, U1026 or Wortmannin (**Figure 4E and Supplementary Figure 6B**).

In addition, HDGF contributed to the suppression of MMS-induced apoptosis of PSCs. Additionally, the results suggest that CEBPD and HIF-1α mediated TGF-β1-induced HDGF expression. We therefore assessed whether both CEBPD and

HIF-1α played an anti-apoptotic role in TGF-β1-treated PSCs upon MMS treatment. In the absence of CEBPD or HIF-1α in PSCs (**Supplementary Figure 5**), TGF-β1 failed to suppress MMS-induced sub-G1 population of cell cycle and caspase 3/7 activity (**Supplementary Figure 7**).

HDGF and CEBPD expression is positively associated with severely stromal growth in human pancreatic cancer specimens.

The data suggest that the TGF-β1-activated CEBPD/HIF-1α/HDGF axis contributes to anti-apoptotic and pro-fibrotic effects in PSCs and mediates the interplay between PSCs and PCCs. We next assessed the clinical relevance of COL1A2, HDGF, and CEBPD expression using a commercial tissue array. According to cell proportion ratio of stromal cells versus total tissue cells, 78 human primary pancreatic cancer specimens were subdivided into mildly (<50%) or severely (≥50%) stromal growth. After the expression levels of COL1A2, HDGF, and CEBPD were determined in 78 human pancreatic cancer specimens using immunofluorescence staining, histochemistry-score (H-score) method assigned a score of 0-300 to each specimen for assessing the extent of immunoreactivity by an expert pathologist. COL1A2 expression showed strong association ($P<0.001$) with severely stromal growth (**Figure 5A left and 5B**). We also observed significant association between severely stromal growth and high HDGF or

CEBPD expression (**Figure 5A middle**; **Figure 5C**, $P<0.038$; **Figure 5D**, $P<0.042$). According to Tumor/Node/Metastasis staging of pathological verification., 78 pancreatic cancer specimens were subdivided into two groups: stage I (group 1) and stages II, III, and IV (group 2). The H-scores of COL1A2, HDGF, and CEBPD showed a similarity between these two TNM staging groups. (**Figure 5Eto 5G**; NS stands for not significant). We observed that the H-scores of COL1A2, HDGF, and CEBPD showed no significant variation in these two groups (**Figure 5E to 5G**). These results support that HDGF and CEBPD contribute to pro-fibrosis.

DISCUSSION

The aim of the present study was to determine HDGF regulation and function in PSCs as well as to determine its contribution to fibrosis-associated pancreatic cancer. The results demonstrate that TGF-β1 activated HDGF expression through the non-SMAD signaling(s)-activated CEBPD/HIF-1α axis in PSCs. Increased production of HDGF prevented apoptosis and promoted the production of ECM proteins, including COL1A2 and FN1 (**Figure 6**). Importantly, these results suggest that HDGF exerted a pro-fibrotic effect to orchestrate fibrotic architecture and attenuated the penetration of blood vessels, acting as a fibrotic hypo-vascular barrier.

The evidence of HDGF auto-regulation and contribution to cell proliferation and tumorigenesis has been suggested in several types of cancers (Kishima et al., 2002, Song, Cong et al., 2017, Yang, Li et al., 2013). In the present study, we determined that regulation of HDGF in PSCs contributed to fibrosis (**Figure 1G and Figure 2**) and demonstrated the smaller and separated sphere formation of PCCs in co-cultures with *shHDGF* PSCs (**Figure 1H and 1I**). This result supports the role of HDGF in benefiting cancer progression and directly suggests the involvement of stromal HDGF in promoting cancer cell proliferation. Therefore, in addition to clarifying the individual contribution of HDGF from cancer cells and the stromal cells surrounding cancer cells, the most important issue should be to verify how to use our understanding of HDGF for diagnosis

and cancer therapy.

PSCs not only synthesize ECM proteins (Apte et al., 2012) but also provide pro-survival signals to tumors (Habisch et al., 2010, Masamune & Shimosegawa, 2009). Our results showed that HDGF down-regulation in PSCs orchestrate less or looser the fibrotic architecture in the co-implantation of PCCs and PSCs xenograft model (**Figure 2**). Interestingly, the signals of COL1A2 and FN1 were also observed in GFP-positive EGFP/PANC-1 or EGFP/MIA PaCa-2 cells in tissue sections (**Figure 2C to 2F**). Previous studies have discovered that pancreatic cancer cells express COL1A2 and FN1 (Lohr, Trautmann et al., 1994) and are able to take up collagen fragments from stromal microenvironment under nutrient limited conditions (Olivares, Mayers et al., 2017). We proposed that the accumulation of COL1A2 and FN1 in pancreatic cancer cells could be resulted from above machinery. However, how stromal HDGF affects the cancerous expression of extracellular matrix proteins remains unrevealed.

Remarkably, fibrosis occurred in each TNM stage of pancreatic cancer (**Figure 5E**); no positive correlation was observed between the stromal HDGF or CEBPD expression levels and malignancies of pancreatic cancers at various TNM stages (**Figure 5F and 5G**), suggesting that the fibrotic involvement of HDGF or CEBPD in the development of pancreatic cancer starts from an early stage under normoxic conditions. A previous study suggested that precise quantitation of the fibrosis levels in pancreatic cancer should be

combined to determine the stage of the disease, select optimal therapies, and monitor or predict patient therapeutic outcomes (Li, Zhang et al., 2013). The results of the present study suggest that HDGF and CEBPD contribute to the interplay of PSCs and PCCs in pancreatic cancer progression via PSC activation and ECM protein production, thereby indicating that HDGF or CEBPD can serve as a biomarker to evaluate the fibrotic status of pancreatic cancer for the diagnostic assistant of the TNM staging.

TGF-β1 has been demonstrated to be a master regulator in hepatic, renal, and pulmonary fibrosis through SMAD-based signaling pathways (Kao et al., 2010, Meng et al., 2016, Wang, Nie et al., 2013). To our knowledge, this study is the first to demonstrate that CEBPD contributes to PSC activation, particularly in pancreatic cancer progression. We further revealed that the non-SMAD pathways P38, MAPK/ERK, and AKT/PI3K activate CEBPD expression in TGF-β1-treated PSCs. In addition to the SMAD pathway, these observations imply that the non-SMAD pathways P38, MAPK/ERK and AKT/PI3K also contribute to TGF-β1-induced pancreatic fibrosis.

Targeting tumors is currently a major tumor therapeutic strategy. Accumulating studies have highlighted the importance of the tumor microenvironment in benefiting cancer progression (Neesse, Algul et al., 2015, Tod, Jenei et al., 2013, Wilson, Pirola et al., 2014). However, the critical and central genes involved in the interplay of cancer and stromal cells remain unknown and their targeting therapies have not been identified. The

results of the present study demonstrate that HDGF is involved in activation of PSCs during fibrosis and architecture of pancreatic cancer tissue via the CEBPD/HIF-1α axis. However, two previous studies demonstrated that depletion of α-SMA-positive fibroblasts (Ozdemir et al., 2014) and loss of sonic hedgehog protein (Rhim et al., 2014) reduce fibrotic reactions and accelerate tumor progression, including enhanced tumor growth and angiogenesis, in undifferentiated and invasive tumors with reduced animal survival. Therefore, in the future, application of therapeutic strategies targeting CEBPD or HDGF in PSCs for reducing fibrotic reactions should be combined with chemotherapeutic drugs to kill pancreatic cancer cells.

MATERIALS AND METHODS

Cell culture

Two human pancreatic cancer cell (PCC) lines, PANC-1 and MIA PaCa-2, and human pancreatic stellate cells (PSCs) were generously provided from Dr. Kelvin K.-C. Tsai (National Health Research Institutes, Taiwan). Both PCCs were cultured with RPMI-1640 medium (GE Healthcare Life Sciences, Logan, Utah, United States; Hyclone, #SH30011.02). PSCs cells were maintained in Dulbecco's Modified Eagle's medium (Life Technologies Co. Ltd., Grand Island, New York, United States; Gibco, #12900-082). Phoenix™ ampho cells (purchased from Allele Biotechnology, San Diego, California, United States; #ABP-RVC-10001) for lenti-virus production were also maintained in Dulbecco's Modified Eagle's medium. All culture media contained 10% fetal bovine serum (Life Technologies Co. Ltd., Grand Island, New York, United States; Gibco, #10437-028) and penicillin-streptomycin solution (Mediatech, Inc., Manassas, Virginia, United States; Corning, #30-002-CI).

Recombinant human TGF-β1, HDGF and chemical inhibitor reagents

Recombinant human TGF-β1 was purchased from the PeproTech, Inc. (Rocky Hill, New Jersey, United States; #100-21C). Recombinant human HDGF was kindly provided from Professor Ming-Hong Tai (National Sun Yat-sen University, Taiwan). The protein synthesis inhibitor (cycloheximide, #C7698) and SMAD inhibitor (SMAD2/3 inhibitor:

SB431542, #S4317) were purchased from Sigma-Aldrich Co. (Saint Louis, Missouri, United States). The non-SMAD inhibitors, including P38 catalytic activity inhibitor (SB203580, #559389), AKT/PI3K inhibitor (Wortmannin, # 681675), and ERK1/2 inhibitor (U0126, #662005), were obtained from Calbiochem (Merck KGaA, Darmstadt, Germany).

Reverse transcription polymerase chain reaction (RT-PCR) assay

Total RNA was extracted from cells using TRIsure™ reagent (Bioline GmbH, Luckenwalde, Germany; #BIO-38033), and the RNA concentration was measured based on the absorbance at 260 nm using a Titertek-Berthold Colibri-Microvolume-Spectrometer (Berthold Detection Systems GmbH, Pforzheim, Germany). cDNA was generated from 1 μg of RNA using SuperScript® III Reverse Transcriptase according to the manufacturer's instructions (Invitrogen Co., Carlsbad, California, United States; #18080085). The specific primer sequences of target gene amplification and reaction conditions are listed at **Supplementary Table 1**. For confirmation, the PCR product was electrophoresed on an agarose gel containing 100 mg/mL ethidium bromide.

Protein extraction and western blot assays

Total proteins were extracted from cells using lysis buffer (10 mM of Tris-HC1 with pH 7.5, 150 mM of NaCl, 5 mM of EDTA, 5 mM of NaN_3, 10 mM of sodium

pyrophosphate, and 1% of Triton X-100). Subsequently, total proteins were separated using 8~15% polyacrylamide-sodium dodecyl sulfate gel. After total proteins were transferred onto an Immobilon®-P Transfer Membrane (Merck KGaA, Darmstadt, Germany; Millipore, #IPVH00010), the membrane was hybridized with a primary antibody (**Supplementary Table 2**) at 4°C overnight and a suitable secondary antibody (**Supplementary Table 2**) at room temperature for one hour. Finally, the UVP BioSpectrum 815 imaging system (UVP, LLC., Upland, California, United States) was used to detect the immunoreactivity of immune complexes after the membrane was incubated with Immobilon™ Western Chemiluminescent horseradish peroxidase substrate (Merck KGaA, Darmstadt, Germany; Millipore, #WBKLS0500).

MTT assay for cell viability analysis

1×10^4 of PSCs were seeded into 24-well plate and treated with or without TGF-β1 (0.5 ng/mL) for 24 hours, and then MTT assay was performed to measure its effect on cell proliferation. 200 μL of thiazolyl blue tetrazolium bromide, MTT (Sigma-Aldrich Co., Saint Louis, Missouri, United States; #M5655), with 0.5 mg/mL was added into each well and incubated for 4 hours. At the end of incubation, 500 μL of dimethyl sulfoxide per well was added to dissolve purple formazen and 200 μL of per well solution transferred into 96-well plate (Twentyman & Luscombe, 1987). The absorbance value at OD 595 nm was measured. The cell viability was calculated using the following formula: % cell viability =

A595 of cells with or without TGF-β1/A595 of control cells without TGF-β1. The cell viability of PSCs without TGF-β1 was normalized to 100% as the control group.

Propidium iodide (PI) staining for apoptosis analysis by flow cytometry

Methyl methanesulfonate (MMS; Sigma-Aldrich Co., Saint Louis, Missouri, United States; #129925) was used to induce cell death through apoptosis. Treated cells were fixed with 70% ethanol overnight and stained with propidium iodide (Sigma-Aldrich Co., Saint Louis, Missouri, United States; #P4170) to stain nuclear DNA at room temperature in the dark (thirty minutes). Using flow cytometry, a Cell Lab Quanta SC (Beckman Coulter, Inc., Brea, California, United States), 10,000 stained cells were acquired. The sub-G1 phase distribution, which indicated the apoptotic cell population, was analyzed on stained cells.

Caspase-3/7activity for apoptosis analysis

After the medium of treated cells was removed, CellEvent™ caspase-3/7 green detection reagent (Thermo Fisher Scientific, Inc., Carlsbad, California, United States; Invitrogen, #C10423) was diluted into complete medium to a final concentration of 2 μM and incubated with treated cells at 37°C in dark for thirty minutes (final sample volume: 100 uL). Subsequently, the fluorogenic response was detected using Labsystems Finstruments 374 Fluoroskan Ascent Fluorescence microplate fluorometer and luminometer (Finland) with an excitation/emission of 485/538 nm.

Lentiviral shRNA system

Expression vectors (pLKO AS3w.puro and pLKO AS3w.eGFP.puro) and other target genes of shRNAs were purchased from the National RNAi Core Facility Platform of Academia Sinica in Taiwan, and the sequences are listed in **Supplementary Table 3**. Additionally, the *mCherry* fluorescent gene was inserted into the *Nhe*1 and *Pme*1 sites of the pLKO AS3w.puro vector. For lentivirus production, the expression vectors or shRNAs were transfected into Phoenix™ ampho cells using TransIT®-2020 Transfection reagent (Mirus Bio LLC., Madison, Wisconsin, United States) according to the manufacturer's instructions. The lentivirus was purified, and the cells were transfected with the target genes of siRNAs using a lentivirus-based system according to the protocol on the website of the National RNAi Core Facility Platform of Academia Sinica. After lenti-viral infection, the cell lysate was extracted for western blot analysis or cells were subjected to fluorescence microscopy to determine the protein expression of the target gene. Subsequently, stable cell lines containing over-expressed or knocked-down target genes were established through antibiotics selection for subsequent experiments. In addition, cells with *shHDGF* or *shLacZ* (as a control group) were further transfected with the *mCherry* fluorescence gene. The method of limiting cell dilution was used to acquire monoclonal cells with the *mCherry* fluorescence gene.

Hanging drop cell culture for three-dimension co-culture system of PSCs and PCCs

PANC-1 cells and MIA PaCa-2 cells were forced to express enhanced green fluorescence protein (EGFP). Subsequently, 2×10^4 EGFP-bearing PANC-1 cells (EGFP/PANC-1) or EGFP-bearing MIA PaCa-2 cells (EGFP/MIA PaCa-2) were individually mixed with 1×10^5 mCherry-bearing *shLacZ* PSCs (mCherry/*shLacZ* PSCs) or mCherry-bearing *shHDGF* PSCs (mCherry/*shHDGF* PSCs). The final volume of mixed cells was 400 μL, containing 50% matrigel matrix (Discovery Labware, Inc., Bedford, Massachusetts, United States; Corning, #356227). Several drops of the mixed cells were seeded onto 35 mm microplate with a glass bottom (ibidi GmbH, Martinsried, Germany; #81158) using hanging drop cell culture to generate a three-dimensional co-culture system. After 8 days, the mixed cells were observed using an Olympus FV1000 confocal microscope (Olympus Co., Shinjuku-ku, Tokyo, Japan) at 100 × magnification. Finally, the fluorescence intensity of the captured images was used to construct the three-dimensional structure according to the z-axis of the captured images using ImageJ software (National Institutes of Health, United States).

Transcription factor prediction

The 2000 bases of the promoter sequences (upstream bases from -2000 to -1 before transcript start site) of HIF-1α and CEBPD were acquired from the University of California Santa Cruz Genome Browser. The promoter sequence was analyzed using the

TFSEARCH (version 1.3) and PROMO server (version 3.0.2), for transcription factor prediction. All the University of California Santa Cruz Genome Browser, TFSEARCH (version 1.3), and PROMO server (version 3.0.2) are open database sources. The predicted transcription factors were further verified using luciferase reporter and chromatin immunoprecipitation (ChIP) assays.

Plasmid transfection

Human HIF-1α expressing vector (pCEP4/HIF-1α; American type Culture Collection, Manassas, Virginia, United States; #MBA-2) was a generous gift from Professor Shaw-Jenq Tsai (National Cheng Kung University (NCKU), Taiwan) (Chien, Lin et al., 2008). Furthermore, the pcDNA3/HA-CEBPD expressing vector was established previously described (Lai, Wang et al., 2008). Plasmids were transfected into cells using the Turbofect™ Transfection reagent (Thermo Fisher Scientific, Inc., Rockford, Illinois, United States; #R0532). Subsequently, the cell lysate was extracted and subjected to western blot analysis to determine the protein expression of the target gene.

Reporter plasmid construction and luciferase reporter assay

Two promoter fragments of the human *HDGF* gene cloned into pGL3-Enhancer vectors (pHDGF 2047: -2017 to +30 and pHDGF 876: -774 to +102) were kindly provided from Professor Ming-Hong Tai (National Sun Yat-sen University, Taiwan). In addition, we also designed appropriate primers to generate two promoter fragments of the

human *HIF-1α* gene; the primer sequences are listed in **Supplementary Table 4**. Briefly, genomic DNA was extracted from cells using the GeneJET™ Genomic DNA Purification Kit (Thermo Fisher Scientific, Inc., Waltham, Massachusetts, United States; Fermentas, #K0722) and used as a template to generate promoter fragments of the target genes using PCR. The promoter fragments of the *HIF-1α* gene were subsequently cloned into pGL3-Basic vectors (Promega Co., Madison, Wisconsin, United States; #E1751). After verification by sequencing, the pGL3-Enhancer vectors bearing promoter fragments of the *HDGF* gene or pGL3-Basic vectors bearing promoter fragments of the *HIF-1α* gene were transfected into cells using the Turbofect™ Transfection reagent. Subsequently, the cell lysate was extracted and analyzed using a luciferase assay system.

Chromatin immunoprecipitation (ChIP) assay

ChIP assay was used to orchestrate protein-DNA interactions. Briefly, the crosslink between DNA and associated proteins on chromatin in living cells was fixed using 1% formaldehyde and neutralized using 1.375 M Glycine. Subsequently, DNA-protein complexes (chromatin-protein) were broken, and DNA fragments shorter less than 1000 base pairs were generated using the Misonix Sonicator 3000 Ultrasonic Cell Disruptor (Misonix, Inc., Farmingdale, New York, United States). The cross-linked DNA fragments associated with protein were selectively immuno-precipitated using primary antibodies as listed in **Supplementary Table 2** and Protein A Agarose/Salmon Sperm DNA beads

(Merck KGaA, Darmstadt, Germany; Upstate, #16-157). The associated DNA fragments were purified and subjected to PCR using the appropriate primers as listed in **Supplementary Table 5** for putative protein binding motifs. Finally, the PCR product was confirmed using agarose gel electrophoresis with ethidium bromide staining.

Animal xenograft model for co-implantation of PSCs and PCCs

The animal experiments were approved by the Institutional Animal Care and Use Committee of NCKU. Non-obese diabetic-severe combined immunodeficiency (NOD-SCID) mice were acquired and maintained in the specific pathogen-free environment at the Laboratory Animal Center of College of Medicine of NCKU. *shLacZ* or *shHDGF* PSCs were individually mixed with EGFP-bearing PANC-1 or EGFP-bearing MIA PaCa-2 cells (each at 1×10^6 cells/50 μL). The mixed cells were added to 100 μL of matrigel matrix (final concentration: 50%; total final volume: 200 μL) and subcutaneously injected into the right flank of 7-week old NOD-SCID mice. After the co-inoculation of PSCs and PCCs for nine weeks, mice were sacrificed. Subcutaneous tumor tissues were dissected and sent to the Human Biobank Research Center of Clinical Medicine of NCKU Hospital for fixing, paraffin-embedding and sectioning. The 4-μm sections of paraffin-embedded tumor tissues were applied for the following experiments.

Picrosirius red staining for collagen analysis

Sirius red stain is specific with respect different extracellular matrix proteins and

materials, such as collagens, laminin, fibronectin, chondroitin sulfate, dermatan sulfate, and amyloid β (Tullberg-Reinert & Jundt, 1999). After the tissue sections were de-paraffinized, a Picrosirius red stain kit (Abcam plc., Cambridge, United Kingdom; #ab150681) was used to stain collagen expression in tumor sections according to the manufacturer's instructions. Images of the collagen histology were visualized and captured using an OLYMPUS DP70 microscope.

Immunohistochemistry (IHC) analysis

All tissue sections were de-paraffinized in 100% xylene and a gradient alcohol concentration. The Novolink™ Polymer Detection Systems Kit (Leica Biosystems Newcastle Ltd., Benton, Lane, Newcastle Upon Tyne, United Kingdom; #RE7140-K) was used to perform IHC analysis according to the manufacturer's instructions. Antigen retrieval was performed in Tris-EDTA buffer at 95°C for fifteen minutes. Subsequently, the tissue sections were incubated with primary antibody at 4°C overnight. The dilutions of the primary antibodies depended on the antigen and are listed in **Supplementary Table 2**. The peroxidase activity was developed using a DAB working solution. Finally, hematoxylin solution (Sigma-Aldrich Co., Saint Louis, Missouri, United States; #HHS32) was used for counter-staining. All images of the tissue sections were observed and captured using an OLYMPUS DP70 microscope.

Immunofluorescence (IF) analysis

Cells and 4-μm of the paraffin-embedded mouse sections were used for IF analysis. Cells were fixed with 4% paraformaldehyde. After the tissue sections were de-paraffinized, Tris-EDTA buffer (10 mM Tris, 1 mM EDTA, and 0.05% Tween 20, pH 9) was used to perform antigen retrieval at 95°C for fifteen minutes. The primary and secondary antibodies were diluted depending on the various antigens listed in **Supplementary Table 2**. Subsequently, fixed cells or de-paraffinized mouse tissue sections were incubated with primary antibody at 4°C overnight and a suitable fluorescence secondary antibody at room temperature in dark for 1 hour. Finally, Hoechst 33258 (Sigma-Aldrich Co., Saint Louis, Missouri, United States; #861405) was used for nuclear DNA staining. Phalloidin-TRITC labeled (Sigma-Aldrich Co., Saint Louis, Missouri, United States; #77418) was also applied for filamentous actin (F-actin) staining on fixed cells for 1 hour. The reagent of ProLong™ diamond antifade mountant with DAPI (Thermo Fisher Scientific, Inc., Waltham, Massachusetts, United States; Life technologies, #P36962) was used for nuclear DNA staining and cell mounting. Finally, images of the cells or tissue sections were observed and captured using an Olympus DP70 microscope or FV10i confocal microscope (Olympus Co., Shinjuku-ku, Tokyo, Japan).

Additionally, the Opal™ multiplex tissue staining kit (PerkinElmer, Inc., Boston, Massachusetts, United States; #NEL794001KT) was applied for IF analysis of a commercial tissue array with 78 human primary pancreatic adenocarcinoma specimens

(purchased from US Biomax, Inc., Derwood, Maryland, United States; # PA961b). The primary and secondary antibodies were diluted depending on the antigens and are listed in **Supplementary Table 2**. The fluorescent intensity and positive staining cell proportion of total cells were evaluated by an expert pathologist (CFL) and presented as a corresponding histochemistry score (H-score) as previously described (Rezaeian, Li et al., 2017). Briefly, H-score method for assessing the extent of immunoreactivity assigns a score of 0-300 to each patient. Experiments performed on human samples were approved by the institutional review board of Chi Mei Medical Center (10606-E03).

Statistical analysis

GraphPad Prism 5 software (GraphPad Software, Inc., La Jolla, California, United States) was used to assess statistical significance using Student's unpaired T-test. The data are presented as the means ± standard error of the mean or median with quartiles. *P* values less than 0.05 were considered statistically significant and are denoted by an asterisk, and NS stands for not significant (*: $P < 0.05$; **: $P < 0.01$; ***: $P < 0.001$; ****: $P < 0.0001$).

ACKNOWLEDGMENTS

This work was financially supported by the National Science Council Grant (NHRI-EX106-10422BI from the National Health Research Institute and MOST 106-2320-B-006-063-MY3 from the Ministry of Science and Technology). We are grateful for the experimental material providing from Professor Shaw-Jenq Tsai (National Cheng Kung University, Taiwan), Dr. Kelvin K.-C. Tsai (National Health Research Institutes, Taiwan), and Professor Ming-Hong Tai (National Sun Yat-sen University, Taiwan).

AUTHOR CONTRIBUTIONS

Y.-T. Chen were responsible to design and perform most of the experiments. Meanwhile, Y.-T. Chen analyzed and interpreted the data and results for writing this manuscript. C.-F. Li performed the clinical human studies and provided helpful suggestions for designing the experiments and editing the manuscript. T.-W. Wang constructed the reporter plasmids, and performed luciferase reporter assays, and assisted with part of immunofluorescence staining assays. T.-H. Chang assisted with the animal studies and the manuscript editing. T.-P. Hsu performed the chromatin immunoprecipitation assays, and assisted with the produce of silencing RNAs and animal studies. J.-Y. Chi and Y.-W. Hsiao cloned *mCherry* fluorescent gene into the pLKO AS3w.puro expression vector. J.-M. Wang directed the project and edited the manuscript.

Conflict of Interest Disclosure: No potential conflicts of interest were to disclose.

REFERENCES

Apte MV, Haber PS, Applegate TL, Norton ID, McCaughan GW, Korsten MA, Pirola RC, Wilson JS (1998) Periacinar stellate shaped cells in rat pancreas: identification, isolation, and culture. Gut 43: 128-33

Apte MV, Pirola RC, Wilson JS (2012) Pancreatic stellate cells: a starring role in normal and diseased pancreas. Front Physiol 3: 344

Bachem MG, Schneider E, Gross H, Weidenbach H, Schmid RM, Menke A, Siech M, Beger H, Grunert A, Adler G (1998) Identification, culture, and characterization of pancreatic stellate cells in rats and humans. Gastroenterology 115: 421-32

Binenbaum Y, Na'ara S, Gil Z (2015) Gemcitabine resistance in pancreatic ductal adenocarcinoma. Drug resistance updates : reviews and commentaries in antimicrobial and anticancer chemotherapy 23: 55-68

Burris HA, 3rd, Moore MJ, Andersen J, Green MR, Rothenberg ML, Modiano MR, Cripps MC, Portenoy RK, Storniolo AM, Tarassoff P, Nelson R, Dorr FA, Stephens CD, Von Hoff DD (1997) Improvements in survival and clinical benefit with gemcitabine as first-line therapy for patients with advanced pancreas cancer: a randomized trial. Journal of clinical oncology : official journal of the American Society of Clinical Oncology 15: 2403-13

Chen SC, Kung ML, Hu TH, Chen HY, Wu JC, Kuo HM, Tsai HE, Lin YW, Wen ZH, Liu JK, Yeh MH, Tai MH (2012) Hepatoma-derived growth factor regulates breast cancer cell invasion by modulating epithelial--mesenchymal transition. J Pathol 228: 158-69

Chi JY, Hsiao YW, Li CF, Lo YC, Lin ZY, Hong JY, Liu YM, Han X, Wang SM, Chen BK, Tsai KK, Wang JM (2015) Targeting chemotherapy-induced PTX3 in tumor stroma to prevent the progression of drug-resistant cancers. Oncotarget 6: 23987-4001

Chien CW, Lin SC, Lai YY, Lin BW, Lin SC, Lee JC, Tsai SJ (2008) Regulation of CD151 by hypoxia controls cell adhesion and metastasis in colorectal cancer. Clinical cancer research : an official journal of the American Association for Cancer Research 14: 8043-51

Chuang CH, Wang WJ, Li CF, Ko CY, Chou YH, Chuu CP, Cheng TL, Wang JM (2014) The combination of the prodrugs perforin-CEBPD and perforin-granzyme B efficiently enhances the activation of caspase signaling and kills prostate cancer. Cell Death Dis 5: e1220

Enomoto H, Nakamura H, Liu W, Nishiguchi S (2015) Hepatoma-Derived Growth Factor: Its Possible Involvement in the Progression of Hepatocellular Carcinoma. Int J Mol Sci 16: 14086-97

Erkan M, Reiser-Erkan C, Michalski CW, Deucker S, Sauliunaite D, Streit S, Esposito I, Friess H, Kleeff J (2009) Cancer-stellate cell interactions perpetuate the hypoxia-fibrosis

cycle in pancreatic ductal adenocarcinoma. Neoplasia 11: 497-508
Habisch H, Zhou S, Siech M, Bachem MG (2010) Interaction of stellate cells with pancreatic carcinoma cells. Cancers 2: 1661-82
Hsiao YW, Li CF, Chi JY, Tseng JT, Chang Y, Hsu LJ, Lee CH, Chang TH, Wang SM, Wang DD, Cheng HC, Wang JM (2013) CCAAT/enhancer binding protein delta in macrophages contributes to immunosuppression and inhibits phagocytosis in nasopharyngeal carcinoma. Sci Signal 6: ra59
Kao YH, Chen CL, Jawan B, Chung YH, Sun CK, Kuo SM, Hu TH, Lin YC, Chan HH, Cheng KH, Wu DC, Goto S, Cheng YF, Chao D, Tai MH (2010) Upregulation of hepatoma-derived growth factor is involved in murine hepatic fibrogenesis. J Hepatol 52: 96-105
Kishima Y, Yamamoto H, Izumoto Y, Yoshida K, Enomoto H, Yamamoto M, Kuroda T, Ito H, Yoshizaki K, Nakamura H (2002) Hepatoma-derived growth factor stimulates cell growth after translocation to the nucleus by nuclear localization signals. J Biol Chem 277: 10315-22
Ko CY, Chang WC, Wang JM (2015) Biological roles of CCAAT/Enhancer-binding protein delta during inflammation. J Biomed Sci 22: 6
Ko CY, Hsu HC, Shen MR, Chang WC, Wang JM (2008) Epigenetic silencing of CCAAT/enhancer-binding protein delta activity by YY1/polycomb group/DNA methyltransferase complex. J Biol Chem 283: 30919-32
Kota J, Hancock J, Kwon J, Korc M (2017) Pancreatic cancer: Stroma and its current and emerging targeted therapies. Cancer Lett 391: 38-49
Krantz SB, Shields MA, Dangi-Garimella S, Cheon EC, Barron MR, Hwang RF, Rao MS, Grippo PJ, Bentrem DJ, Munshi HG (2011) MT1-MMP cooperates with Kras(G12D) to promote pancreatic fibrosis through increased TGF-beta signaling. Molecular cancer research : MCR 9: 1294-304
Lai PH, Wang WL, Ko CY, Lee YC, Yang WM, Shen TW, Chang WC, Wang JM (2008) HDAC1/HDAC3 modulates PPARG2 transcription through the sumoylated CEBPD in hepatic lipogenesis. Biochimica et biophysica acta 1783: 1803-14
Li CF, Tsai HH, Ko CY, Pan YC, Yen CJ, Lai HY, Yuh CH, Wu WC, Wang JM (2015) HMDB and 5-AzadC Combination Reverses Tumor Suppressor CCAAT/Enhancer-Binding Protein Delta to Strengthen the Death of Liver Cancer Cells. Mol Cancer Ther 14: 2623-33
Li W, Zhang Z, Nicolai J, Yang GY, Omary RA, Larson AC (2013) Quantitative magnetization transfer MRI of desmoplasia in pancreatic ductal adenocarcinoma xenografts. NMR in biomedicine 26: 1688-95
Li X, Ma Q, Xu Q, Duan W, Lei J, Wu E (2012) Targeting the cancer-stroma interaction: a potential approach for pancreatic cancer treatment. Current pharmaceutical design 18:

2404-15
Lohr M, Trautmann B, Gottler M, Peters S, Zauner I, Maillet B, Kloppel G (1994) Human ductal adenocarcinomas of the pancreas express extracellular matrix proteins. Br J Cancer 69: 144-51
Majmundar AJ, Wong WJ, Simon MC (2010) Hypoxia-inducible factors and the response to hypoxic stress. Mol Cell 40: 294-309
Masamune A, Kikuta K, Watanabe T, Satoh K, Hirota M, Hamada S, Shimosegawa T (2009) Fibrinogen induces cytokine and collagen production in pancreatic stellate cells. Gut 58: 550-9
Masamune A, Kikuta K, Watanabe T, Satoh K, Hirota M, Shimosegawa T (2008) Hypoxia stimulates pancreatic stellate cells to induce fibrosis and angiogenesis in pancreatic cancer. American journal of physiology Gastrointestinal and liver physiology 295: G709-17
Masamune A, Shimosegawa T (2009) Signal transduction in pancreatic stellate cells. J Gastroenterol 44: 249-60
Masamune A, Watanabe T, Kikuta K, Shimosegawa T (2009) Roles of pancreatic stellate cells in pancreatic inflammation and fibrosis. Clinical gastroenterology and hepatology : the official clinical practice journal of the American Gastroenterological Association 7: S48-54
Meng XM, Nikolic-Paterson DJ, Lan HY (2016) TGF-beta: the master regulator of fibrosis. Nat Rev Nephrol 12: 325-38
Menke A, Adler G (2002) TGFbeta-induced fibrogenesis of the pancreas. Int J Gastrointest Cancer 31: 41-6
Moir JA, Mann J, White SA (2015) The role of pancreatic stellate cells in pancreatic cancer. Surgical oncology 24: 232-8
Nakamura H, Izumoto Y, Kambe H, Kuroda T, Mori T, Kawamura K, Yamamoto H, Kishimoto T (1994) Molecular cloning of complementary DNA for a novel human hepatoma-derived growth factor. Its homology with high mobility group-1 protein. The Journal of biological chemistry 269: 25143-9
Neesse A, Algul H, Tuveson DA, Gress TM (2015) Stromal biology and therapy in pancreatic cancer: a changing paradigm. Gut 64: 1476-84
Olivares O, Mayers JR, Gouirand V, Torrence ME, Gicquel T, Borge L, Lac S, Roques J, Lavaut MN, Berthezene P, Rubis M, Secq V, Garcia S, Moutardier V, Lombardo D, Iovanna JL, Tomasini R, Guillaumond F, Vander Heiden MG, Vasseur S (2017) Collagen-derived proline promotes pancreatic ductal adenocarcinoma cell survival under nutrient limited conditions. Nat Commun 8: 16031
Olive KP, Jacobetz MA, Davidson CJ, Gopinathan A, McIntyre D, Honess D, Madhu B, Goldgraben MA, Caldwell ME, Allard D, Frese KK, Denicola G, Feig C, Combs C,

Winter SP, Ireland-Zecchini H, Reichelt S, Howat WJ, Chang A, Dhara M et al. (2009) Inhibition of Hedgehog signaling enhances delivery of chemotherapy in a mouse model of pancreatic cancer. Science 324: 1457-61
Ooi BN, Mukhopadhyay A, Masilamani J, Do DV, Lim CP, Cao XM, Lim IJ, Mao L, Ren HN, Nakamura H, Phan TT (2010) Hepatoma-derived growth factor and its role in keloid pathogenesis. J Cell Mol Med 14: 1328-37
Ozdemir BC, Pentcheva-Hoang T, Carstens JL, Zheng X, Wu CC, Simpson TR, Laklai H, Sugimoto H, Kahlert C, Novitskiy SV, De Jesus-Acosta A, Sharma P, Heidari P, Mahmood U, Chin L, Moses HL, Weaver VM, Maitra A, Allison JP, LeBleu VS et al. (2014) Depletion of carcinoma-associated fibroblasts and fibrosis induces immunosuppression and accelerates pancreas cancer with reduced survival. Cancer cell 25: 719-34
Rezaeian AH, Li CF, Wu CY, Zhang X, Delacerda J, You MJ, Han F, Cai Z, Jeong YS, Jin G, Phan L, Chou PC, Lee MH, Hung MC, Sarbassov D, Lin HK (2017) A hypoxia-responsive TRAF6-ATM-H2AX signalling axis promotes HIF1alpha activation, tumorigenesis and metastasis. Nat Cell Biol 19: 38-51
Rhim AD, Oberstein PE, Thomas DH, Mirek ET, Palermo CF, Sastra SA, Dekleva EN, Saunders T, Becerra CP, Tattersall IW, Westphalen CB, Kitajewski J, Fernandez-Barrena MG, Fernandez-Zapico ME, Iacobuzio-Donahue C, Olive KP, Stanger BZ (2014) Stromal elements act to restrain, rather than support, pancreatic ductal adenocarcinoma. Cancer cell 25: 735-47
Sada M, Ohuchida K, Horioka K, Okumura T, Moriyama T, Miyasaka Y, Ohtsuka T, Mizumoto K, Oda Y, Nakamura M (2016) Hypoxic stellate cells of pancreatic cancer stroma regulate extracellular matrix fiber organization and cancer cell motility. Cancer letters 372: 210-8
Shih TC, Tien YJ, Wen CJ, Yeh TS, Yu MC, Huang CH, Lee YS, Yen TC, Hsieh SY (2012) MicroRNA-214 downregulation contributes to tumor angiogenesis by inducing secretion of the hepatoma-derived growth factor in human hepatoma. J Hepatol 57: 584-91
Song R, Cong L, Ni G, Chen M, Sun H, Sun Y, Chen M (2017) MicroRNA-195 inhibits the behavior of cervical cancer tumors by directly targeting HDGF. Oncol Lett 14: 767-775
Tod J, Jenei V, Thomas G, Fine D (2013) Tumor-stromal interactions in pancreatic cancer. Pancreatology 13: 1-7
Tullberg-Reinert H, Jundt G (1999) In situ measurement of collagen synthesis by human bone cells with a sirius red-based colorimetric microassay: effects of transforming growth factor beta2 and ascorbic acid 2-phosphate. Histochemistry and cell biology 112: 271-6
Twentyman PR, Luscombe M (1987) A study of some variables in a tetrazolium dye

(MTT) based assay for cell growth and chemosensitivity. Br J Cancer 56: 279-85
Vogelmann R, Ruf D, Wagner M, Adler G, Menke A (2001) Effects of fibrogenic mediators on the development of pancreatic fibrosis in a TGF-beta1 transgenic mouse model. Am J Physiol Gastrointest Liver Physiol 280: G164-72
Vonlaufen A, Phillips PA, Yang L, Xu Z, Fiala-Beer E, Zhang X, Pirola RC, Wilson JS, Apte MV (2010) Isolation of quiescent human pancreatic stellate cells: a promising in vitro tool for studies of human pancreatic stellate cell biology. Pancreatology 10: 434-43
Wang P, Nie X, Wang Y, Li Y, Ge C, Zhang L, Wang L, Bai R, Chen Z, Zhao Y, Chen C (2013) Multiwall carbon nanotubes mediate macrophage activation and promote pulmonary fibrosis through TGF-beta/Smad signaling pathway. Small 9: 3799-811
Wang Z, Li Y, Ahmad A, Banerjee S, Azmi AS, Kong D, Sarkar FH (2011) Pancreatic cancer: understanding and overcoming chemoresistance. Nature reviews Gastroenterology & hepatology 8: 27-33
Wehr AY, Furth EE, Sangar V, Blair IA, Yu KH (2011) Analysis of the human pancreatic stellate cell secreted proteome. Pancreas 40: 557-66
Wilson JS, Pirola RC, Apte MV (2014) Stars and stripes in pancreatic cancer: role of stellate cells and stroma in cancer progression. Front Physiol 5: 52
Yamamoto S, Tomita Y, Hoshida Y, Takiguchi S, Fujiwara Y, Yasuda T, Doki Y, Yoshida K, Aozasa K, Nakamura H, Monden M (2006) Expression of hepatoma-derived growth factor is correlated with lymph node metastasis and prognosis of gastric carcinoma. Clin Cancer Res 12: 117-22
Yang Y, Li H, Zhang F, Shi H, Zhen T, Dai S, Kang L, Liang Y, Wang J, Han A (2013) Clinical and biological significance of hepatoma-derived growth factor in Ewing's sarcoma. J Pathol 231: 323-34

FIGURE LEGENDS

Figure 1. Hepatoma-derived growth factor (HDGF) exerts an anti-apoptotic effect and is required for activation of pancreatic stellate cells (PSCs) that interact with pancreatic cancer cells (PCCs).

(A) PSCs were treated with transforming growth factor-β1 (TGF-β1) in a dose-dependent manner for 24 hours. The markers of activated PSCs, α-smooth muscle actin (α-SMA) and vimentin were further determined using reverse transcription-polymerase chain reaction (RT-PCR) and western blot (WB) assays. (B) Immunofluorescence staining was used to examine the markers of activated PSCs, such as the high expression of α-smooth muscle actin (α-SMA) and filamentous actin (F-actin) rearrangement. α-SMA expression and F-actin rearrangement were determined in PSCs treated with or without 0.5 ng/mL of recombined human TGF-β1 for 24 hours. Immunofluorescence staining images were captured under a vertical fluorescent microscope to observe morphological changes (white scale bar 100 μm). Green and red fluorescence indicate expression of α-SMA and F-actin, respectively. (C) The conditional medium was collected and concentrated from PSCs with or without 0.5 ng/mL of TGF-β1 treatment for 24 hours. Secreted HDGF expression was determined using western blotting assays, and α-tubulin served as a negative control to exclude the signals from PSCs. (D) to (F) Methyl methanesulfonate (MMS)

treatment was used to induce cell death by apoptosis. Treated PSCs were harvested and subjected to an analysis of the cell cycle distribution by flow cytometry using propidium iodide staining. The sub-G1 phase indicated the apoptotic cell population. Cells were pre-treated with indicated recombined human HDGF for 6 hours or TGF-β1 (0.5 ng/mL) for 24 hours. MMS (75 μg/mL) was administered to treated cells for following 24 hours. (G) Expression of α-SMA, type-I collagen (COL1A2), and fibronectin (FN1) was determined in the control (*shLacZ*) and HDGF knockdown (*shHDGF*) PSCs under 0.5 ng/mL of TGF-β1 stimulation for 24 hours by western blot assays. (H) and (I) PSCs were, respectively, transfected with *shLacZ* (as a control group) or *shHDGF*; cells were further transfected with the *mCherry* fluorescent gene. The *shLacZ* or *shHDGF* PSCs expressing mCherry were, respectively, co-cultured with EGFP-bearing PANC-1 or EGFP-bearing MIA PaCa-2 cells. The mixed PSCs and PCCs (ratio = 5:1) were suspended in 50% matrigel and subjected to a three-dimension system by hanging drop cell culture. After 8 days, the sphere structure was observed at 100× magnification and captured at by confocal microscopy (white scale bar 100 μm). According to the z-section of captured images, the fluorescence intensity was remodeled to reconstruct the three-dimension structure by ImageJ software. The above data are presented as the means ± standard error of the mean from three independent experiments, and the statistical significance was

determined using Student's unpaired T-test (* $P < 0.05$; ** $P < 0.01$; *** $P < 0.001$; **** $P < 0.0001$).

Figure 2. HDGF knockdown in PSCs attenuates fibrotic effects that are as a hypo-vascular barrier *in vivo*.

PCCs, PANC-1 and MIA PaCa-2 cells were transfected the enhanced green fluorescent protein (EGFP) gene. *shLacZ* or *shHDGF* PSCs were individually mixed with EGFP-bearing PANC-1 or EGFP-bearing MIA PaCa-2 cells. The mixture of PSCs and PCCs (ratio = 1:1) containing with 50% matrigel was subcutaneously injected into non-obese diabetic-severe combined immunodeficiency mice. Each group contained 5 to 6 mice. After mice were sacrificed at the ninth week, tissue sections of subcutaneous tumors were subjected to immunofluorescence, Picrosirius red staining, and immunohistochemistry analysis. (A) and (B) Picrosirius red stain was applied to evaluate the expression of collagens. The images (left-upper panels) were observed at 100× magnification; the areas bound by the yellow dotted line were observed at 200× magnification under a vertical microscope and the captured images were shown as the right-lower panels (white scale bar 100 μm). Red color indicates positive staining of collagens, which are quantified in the right panels. (C) to (F) Expression of COL1A2, FN1, and green fluorescent protein (GFP) was determined

using immunofluorescence stain. The images were observed at 400× magnification under a vertical microscope (white scale bar 100 μm). GFP expression in the upper panels indicates the locations of PCCs. The white dished line circles the regions of stromal cells that were GFP-negative expression. The mean fluorescence intensity (MFI) of COL1A2 and FN1 in GFP-negative cells are quantified by ImageJ software and shown in the right panels. (G) and (H) Immunohistochemistry assays were also performed to determine the tumor vasculature by staining with the endothelial cell marker CD31. The images were observed at 200× magnification (white scale bar 100 μm); the brown color indicates positive staining of CD31 expression, which is quantified in the right panels. Above results are presented as the means ± standard error of the mean; the statistical significance was determined using Student's unpaired T-test (* $P < 0.05$; ** $P < 0.01$; *** $P < 0.001$; **** $P < 0.0001$).

Figure 3. HDGF is transcriptionally up-regulated by TGF-β1/ Hypoxia inducible factor-1α (HIF-1α)/ CCAAT/enhancer binding protein δ (CEBPD) axis.

(A) After TGF-β1 treatment for 24 hours, the mRNA or protein levels of HDGF and HIF-1α were determined using RT-PCR or western blot assays in PSCs, respectively. (B) The putative HIF-1α binding motifs on *HDGF* promoter region were shown in upper panel. The HDGF reporter vector was transfected into PSCs simultaneously

with the pCEP4/HIF-1α expressing vector (or pcDNA3/HA expressing vector as a control group) for 18 hours; then, a luciferase reporter assay was performed to confirm the putative HIF-1α-binding motifs on *HDGF* promoter region. The results are from three independent experiments and presented as the means ± standard error of the mean; the statistical significance was determined using Student's unpaired T-test (*** $P < 0.001$). (C) A chromatin immunoprecipitation assay was performed to determine the binding of HIF-1α onto the *HDGF* promoter region in PSCs treated with 0.5 ng/mL TGF-β1 for 24 hours. The IgG antibody was used as a negative control. (D) After PSCs were treated with 0.5 ng/mL TGF-β1 for 24 hours, the mRNA or protein expression levels of CEBPD and TGF-β1 were determined using RT-PCR or western blot assays, respectively. (E) A luciferase reporter assay was used to confirm the putative CEBPD-binding motifs on *HIF-1α* promoter region. The putative CEBPD binding motifs on *HIF-1α* promoter region were shown in upper panel. PSCs were transfected with the *HIF-1α* reporter vector and pcDNA3/HA or pcDNA3/CEBPD expressing vectors for 18 hours and subsequently subjected to luciferase reporter assays. The results are presented as the means ± standard error of the mean, and the statistical significance was determined using Student's unpaired t-test (** $P < 0.01$; *** $P < 0.001$). The above data are from three independent experiments. (F) The results of the chromatin immunoprecipitation assays showed the

interaction between CEBPD and the *HIF-1α* promoter in PSCs treated with 0.5 ng/mL TGF-β1 for 24 hours.

Figure 4. CEBPD participates in activation of PSCs through non-SMAD pathways in TGF-β1 signaling.

(A) After PSCs were transfected with pcDNA3/EGFP-CEBPD or the pcDNA/EGFP expression vectors for 18 hours, cells were harvested and subjected to RT-PCR and western blot assays. The mRNA and protein expression levels of α-SMA, CEBPD, HIF-1α, and HDGF were determined in PSCs with or without CEBPD overexpression. (B) In addition, *shLacZ* PSCs (as a control group) and *shCEBPD* PSCs were subjected to RT-PCR and western blot assays to examine the mRNA and protein expression levels of α-SMA, CEBPD, HIF-1α, and HDGF after TGF-β1 treatment for 24 hours. (C) The markers of activated PSCs that could be used to observe morphological changes, such as the high expression of α-SMA and F-actin rearrangement, were determined using immunofluorescence staining in control or CEBPD knockdown PSCs treated with or without 0.5 ng/mL of TGF-β1 for 24 hours (lower panels). The green and red fluorescence indicates expression of α-SMA and F-actin, respectively. In addition, CEBPD expression was evaluated in treated cells using immunofluorescence staining (upper panels). The green and red fluorescence

indicates expression of α-SMA and CEBPD, respectively. The white scale bar indicated 100 μm. (D) and (E) The mRNA and protein levels of CEBPD were determined in *shLacZ* PSCs with co-treatment of TGF-β1 (0.5 ng/mL) and a SMAD inhibitor (SB431542, 10 μM) or non-SMAD inhibitors (P38 catalytic activity inhibitor: SB203580, 5 μM; MAPK/ERK inhibitor: U1026, 5 μM; AKT/PI3K inhibitor: Wortmannin, 100 nM) for 24 hours. The above data are representative from three independent experiments.

Figure 5. HDGF and CEBPD expression is positively associate with stromal overgrowth in human pancreatic cancer specimens.

(A) The Opal™ multiplex tissue staining kit was used for immunofluorescence analysis on a commercial tissue array with 78 human primary pancreatic adenocarcinoma specimens. A ratio of cell proportions from stromal cells versus total tissue cells was determined the 78 human primary pancreatic adenocarcinoma specimens subdivided into mildly (<50%) or severely (<50%) stromal growth. Expression of COL1A2, HDGF, and CEBPD was determined in human pancreatic cancer specimens using immunofluorescence staining and labeled by green, red, and cyan fluorescence, respectively. The white scale bar indicated 100 μm. (B) to (D) Histochemistry-score (H-score), which assigned a score of 0-300 to each patient by an

expert pathologist, is applicable to assess the extent of immunoreactivity of COL1A2 (B), HDGF (C), and CEBPD (D). The expression of COL1A2, HDGF, and CEBPD was significantly and positively associated with stromal overgrowth. The results are presented as both the mean ± standard error of mean and median with quartiles. Student's unpaired T-test was used for comparison between two groups, with $P < 0.05$ taken as indicating a significant difference (* $P < 0.05$; ** $P < 0.01$; *** $P < 0.001$). (E) to (G) According to Tumor/Node/Metastasis (TNM) staging, 78 pancreatic cancer specimens were grouped into two groups: stage I (group 1) and stages II, III, and IV (group 2). The H-scores of COL1A2, HDGF, and CEBPD showed a similarity between these two groups. The results are presented as both of mean ± standard error of mean and median with quartiles. Student's unpaired T-test was used for comparison between two groups, with $P < 0.05$ taken as indicating a significant difference (NS stands for not significant).

Figure 6. A schematic illustration of a signal pathway in pancreatic stellate cells to construct fibrotic architecture.

TGF-β1-activated PSCs secreted HDGF through the TGF-β1/CEBPD/HIF-1α axis. The effects of HDGF in PSCs severed were anti-apoptosis under methyl methanesulfonate stimulation. Additionally, HDGF acted as a pro-fibrotic factor

because its expression was required for activated PSCs to synthesize extracellular matrix proteins, such as type-I collagen and fibronectin. These results suggest roles for HDGF in anti-apoptosis and pro-fibrosis in PSCs. Furthermore, TGF-β1 activated CEBPD through non-SMAD pathways, and TGF-β1 was induced by CEBPD through reciprocal regulation. These results suggest that CEBPD serves as an upstream mediator to regulate PSC activation.

Figure 1

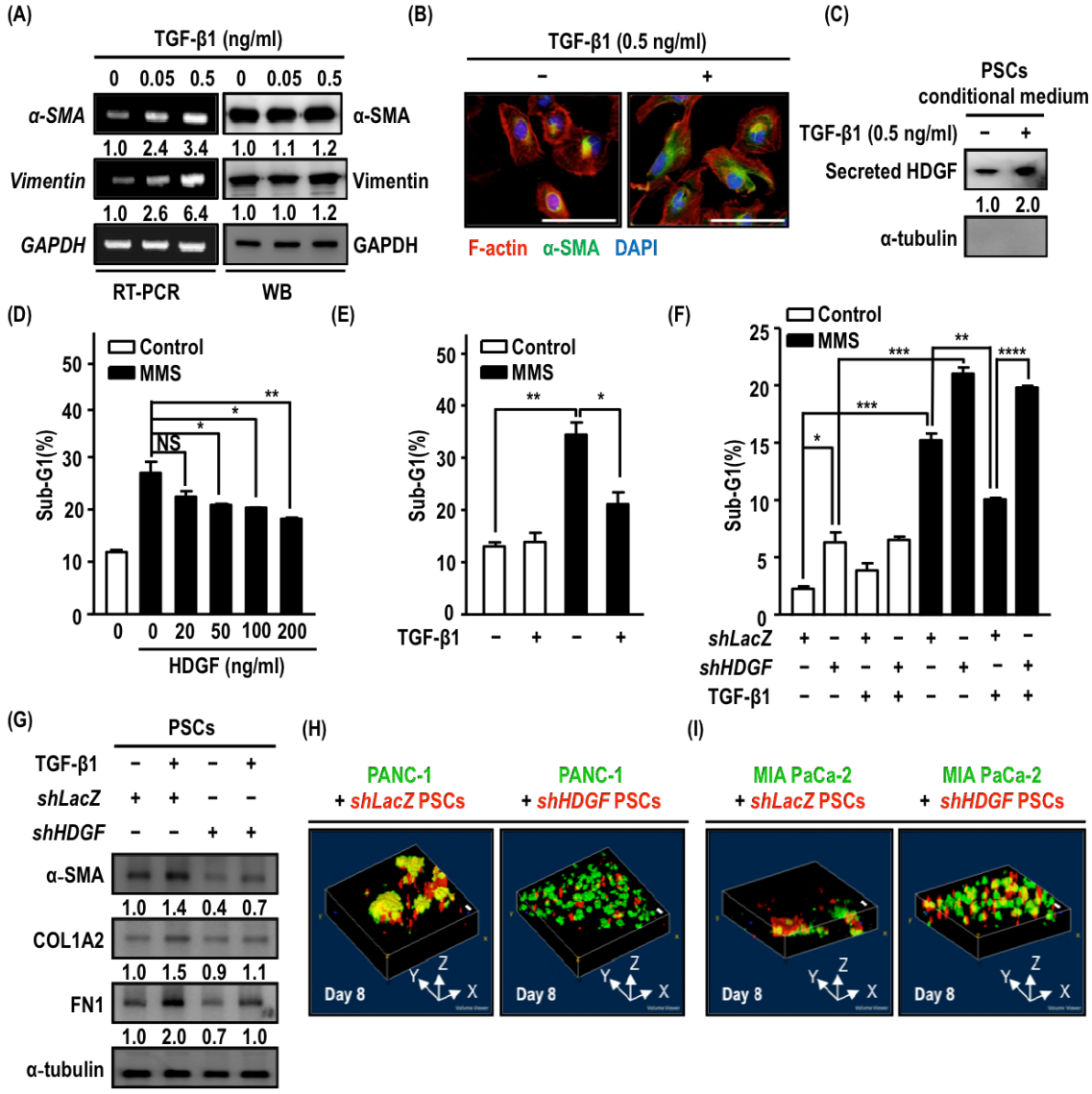
(A)
TGF-β1 (ng/ml)
0 0.05 0.5 0 0.05 0.5
α-SMA
1.0 2.4 3.4 1.0 1.1 1.2
Vimentin
1.0 2.6 6.4 1.0 1.0 1.2
GAPDH
RT-PCR
WB
(B)
TGF-β1 (0.5 ng/ml)
F-actin α-SMA DAPI
(C)
PSCs conditional medium
TGF-β1 (0.5 ng/ml)
Secreted HDGF
1.0 2.0
α-tubulin
(D)
Control
MMS
Sub-G1(%)
HDGF (ng/ml)
(E)
TGF-β1
(F)
shLacZ
shHDGF
TGF-β1
(G)
PSCs
TGF-β1
shLacZ
shHDGF
α-SMA
1.0 1.4 0.4 0.7
COL1A2
1.0 1.5 0.9 1.1
FN1
1.0 2.0 0.7 1.0
α-tubulin
(H)
PANC-1 + shLacZ PSCs
PANC-1 + shHDGF PSCs
(I)
MIA PaCa-2 + shLacZ PSCs
MIA PaCa-2 + shHDGF PSCs
Day 8

Figure 2

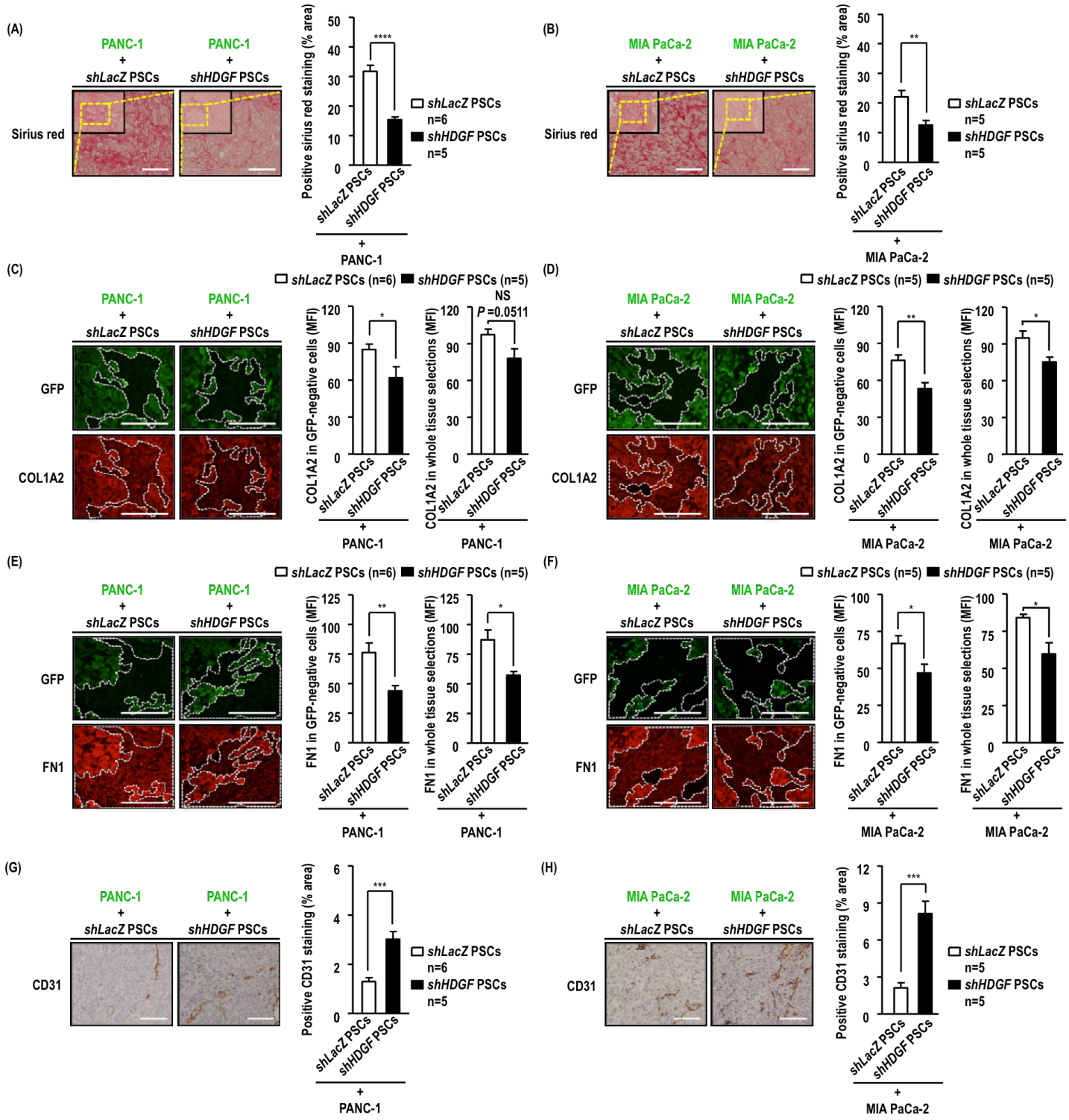
(A)
PANC-1 + shLacZ PSCs
PANC-1 + shHDGF PSCs
Sirius red
Positive sirius red staining (% area)
****
shLacZ PSCs n=6
shHDGF PSCs n=5
+ PANC-1
(B)
MIA PaCa-2 + shLacZ PSCs
MIA PaCa-2 + shHDGF PSCs
Sirius red
Positive sirius red staining (% area)
**
shLacZ PSCs n=5
shHDGF PSCs n=5
+ MIA PaCa-2
(C)
shLacZ PSCs (n=6) shHDGF PSCs (n=5)
GFP
COL1A2
COL1A2 in GFP-negative cells (MFI)
COL1A2 in whole tissue selections (MFI)
NS
P =0.0511
+ PANC-1
(D)
shLacZ PSCs (n=5) shHDGF PSCs (n=5)
+ MIA PaCa-2
(E)
shLacZ PSCs (n=6) shHDGF PSCs (n=5)
FN1
FN1 in GFP-negative cells (MFI)
FN1 in whole tissue selections (MFI)
(F)
shLacZ PSCs (n=5) shHDGF PSCs (n=5)
(G)
CD31
Positive CD31 staining (% area)
***
shLacZ PSCs n=6
shHDGF PSCs n=5
(H)
shLacZ PSCs n=5
shHDGF PSCs n=5

Figure 3

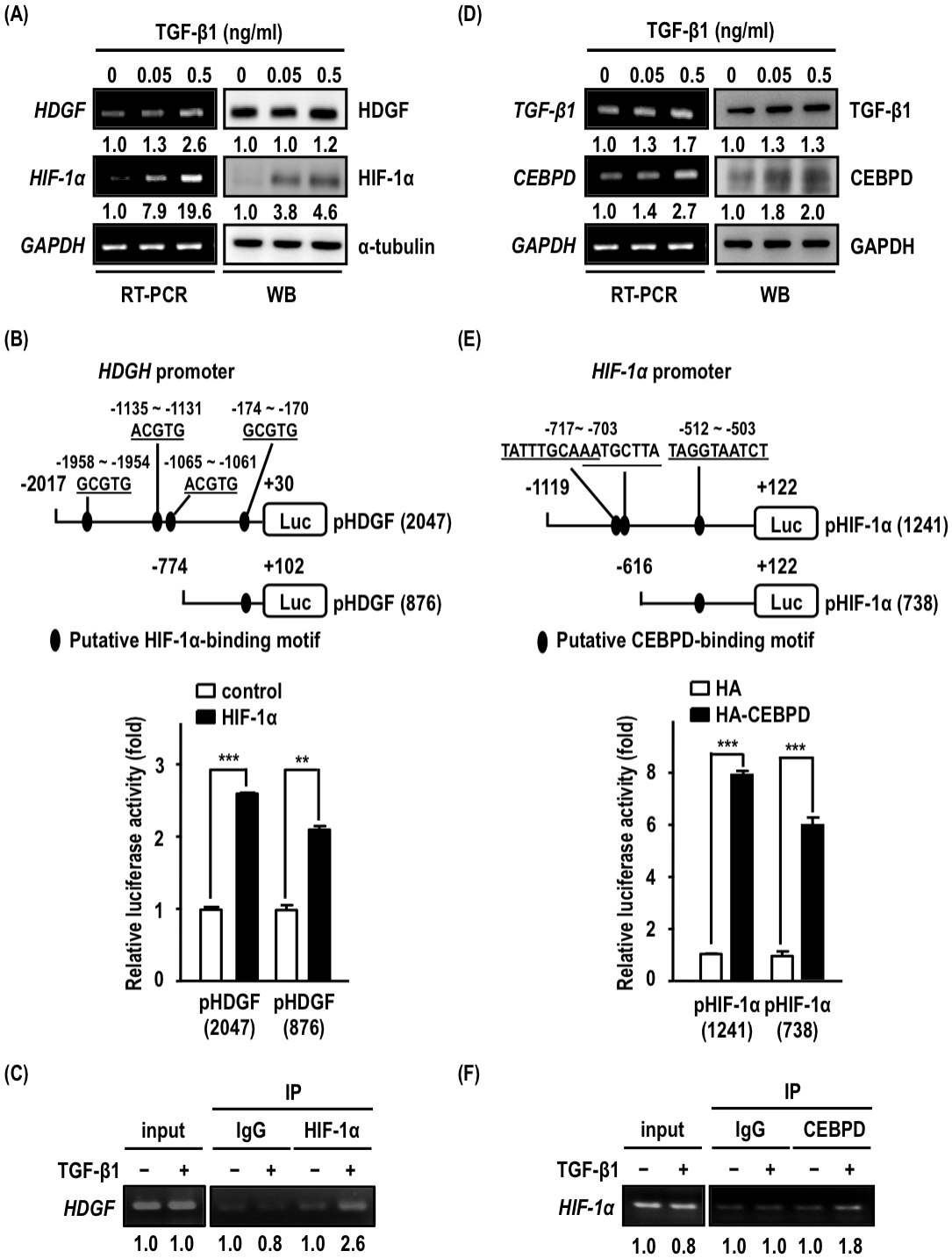
(A)
TGF-β1 (ng/ml)
0 0.05 0.5 0 0.05 0.5
HDGF
HDGF
1.0 1.3 2.6 1.0 1.0 1.2
HIF-1α
HIF-1α
1.0 7.9 19.6 1.0 3.8 4.6
GAPDH
α-tubulin
RT-PCR
WB
(D)
TGF-β1 (ng/ml)
0 0.05 0.5 0 0.05 0.5
TGF-β1
TGF-β1
1.0 1.3 1.7 1.0 1.3 1.3
CEBPD
CEBPD
1.0 1.4 2.7 1.0 1.8 2.0
GAPDH
GAPDH
RT-PCR
WB
(B)
HDGH promoter
-1135 ~ -1131
ACGTG
-174 ~ -170
GCGTG
-1958 ~ -1954
-1065 ~ -1061
-2017 GCGTG
ACGTG
+30
Luc
pHDGF (2047)
-774
+102
Luc
pHDGF (876)
Putative HIF-1α-binding motif
(E)
HIF-1α promoter
-717~ -703
TATTTGCAAATGCTTA
-512 ~ -503
TAGGTAATCT
-1119
+122
Luc
pHIF-1α (1241)
-616
+122
Luc
pHIF-1α (738)
Putative CEBPD-binding motif
control
HIF-1α
Relative luciferase activity (fold)
0
1
2
3
***
**
pHDGF (2047)
pHDGF (876)
HA
HA-CEBPD
Relative luciferase activity (fold)
0
2
4
6
8
***
***
pHIF-1α (1241)
pHIF-1α (738)
(C)
IP
input
IgG
HIF-1α
TGF-β1 − + − + − +
HDGF
1.0 1.0 1.0 0.8 1.0 2.6
(F)
IP
input
IgG
CEBPD
TGF-β1 − + − + − +
HIF-1α
1.0 0.8 1.0 1.0 1.0 1.8

Figure 4

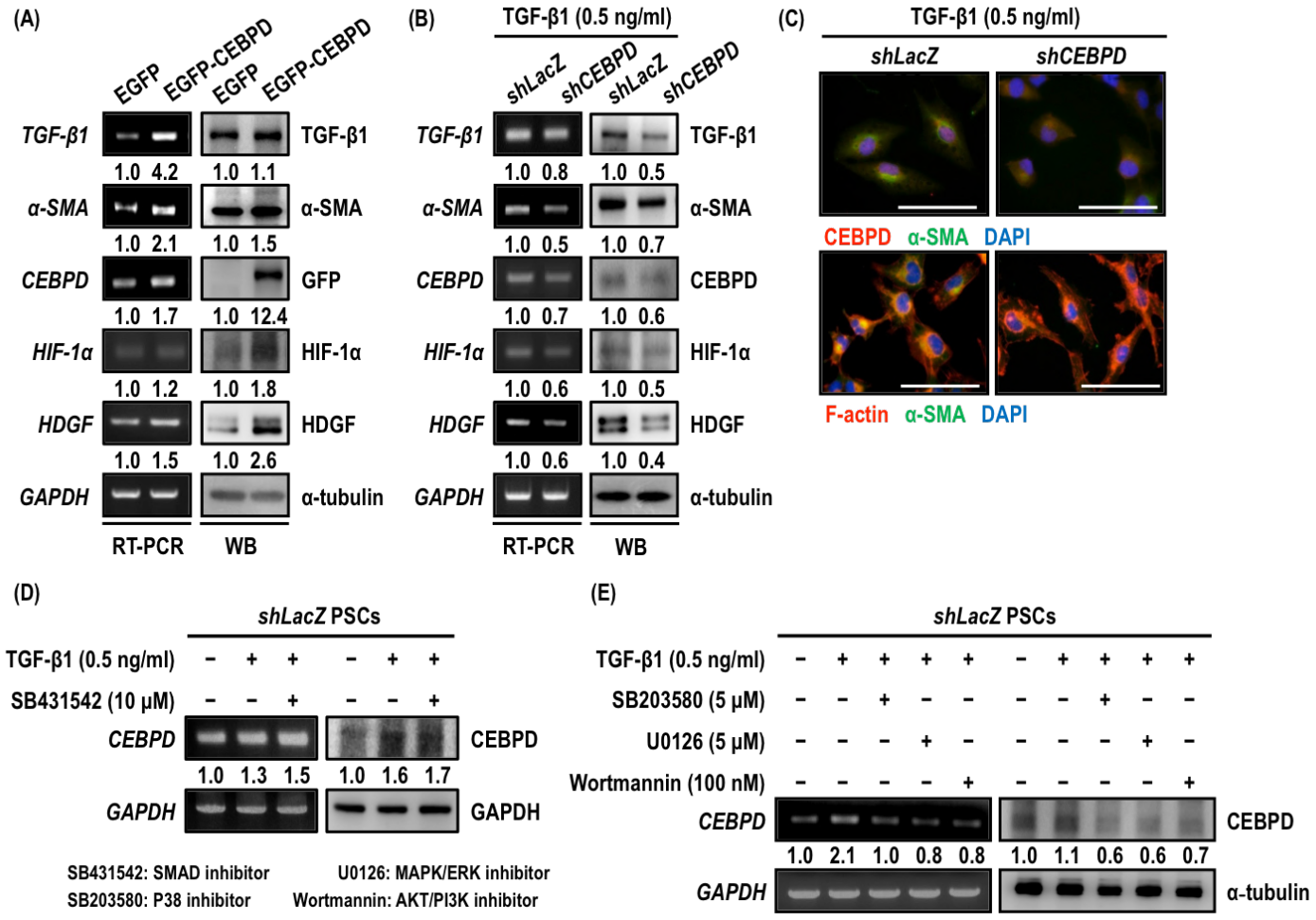
(A)
EGFP
EGFP-CEBPD
EGFP
EGFP-CEBPD
TGF-β1
1.0 4.2
1.0 1.1
TGF-β1
α-SMA
1.0 2.1
1.0 1.5
α-SMA
CEBPD
1.0 1.7
1.0 12.4
GFP
HIF-1α
1.0 1.2
1.0 1.8
HIF-1α
HDGF
1.0 1.5
1.0 2.6
HDGF
GAPDH
α-tubulin
RT-PCR
WB
(B)
TGF-β1 (0.5 ng/ml)
shLacZ
shCEBPD
shLacZ
shCEBPD
TGF-β1
1.0 0.8
1.0 0.5
TGF-β1
α-SMA
1.0 0.5
1.0 0.7
α-SMA
CEBPD
1.0 0.7
1.0 0.6
CEBPD
HIF-1α
1.0 0.6
1.0 0.5
HIF-1α
HDGF
1.0 0.6
1.0 0.4
HDGF
GAPDH
α-tubulin
RT-PCR
WB
(C)
TGF-β1 (0.5 ng/ml)
shLacZ
shCEBPD
CEBPD α-SMA DAPI
F-actin α-SMA DAPI
(D)
shLacZ PSCs
TGF-β1 (0.5 ng/ml) − + + − + +
SB431542 (10 μM) − − + − − +
CEBPD
1.0 1.3 1.5
1.0 1.6 1.7
CEBPD
GAPDH
GAPDH
SB431542: SMAD inhibitor
SB203580: P38 inhibitor
U0126: MAPK/ERK inhibitor
Wortmannin: AKT/PI3K inhibitor
(E)
shLacZ PSCs
TGF-β1 (0.5 ng/ml) − + + + + − + + + +
SB203580 (5 μM) − − + − − − − + − −
U0126 (5 μM) − − − + − − − − + −
Wortmannin (100 nM) − − − − + − − − − +
CEBPD
1.0 2.1 1.0 0.8 0.8
1.0 1.1 0.6 0.6 0.7
CEBPD
GAPDH
α-tubulin

Figure 5

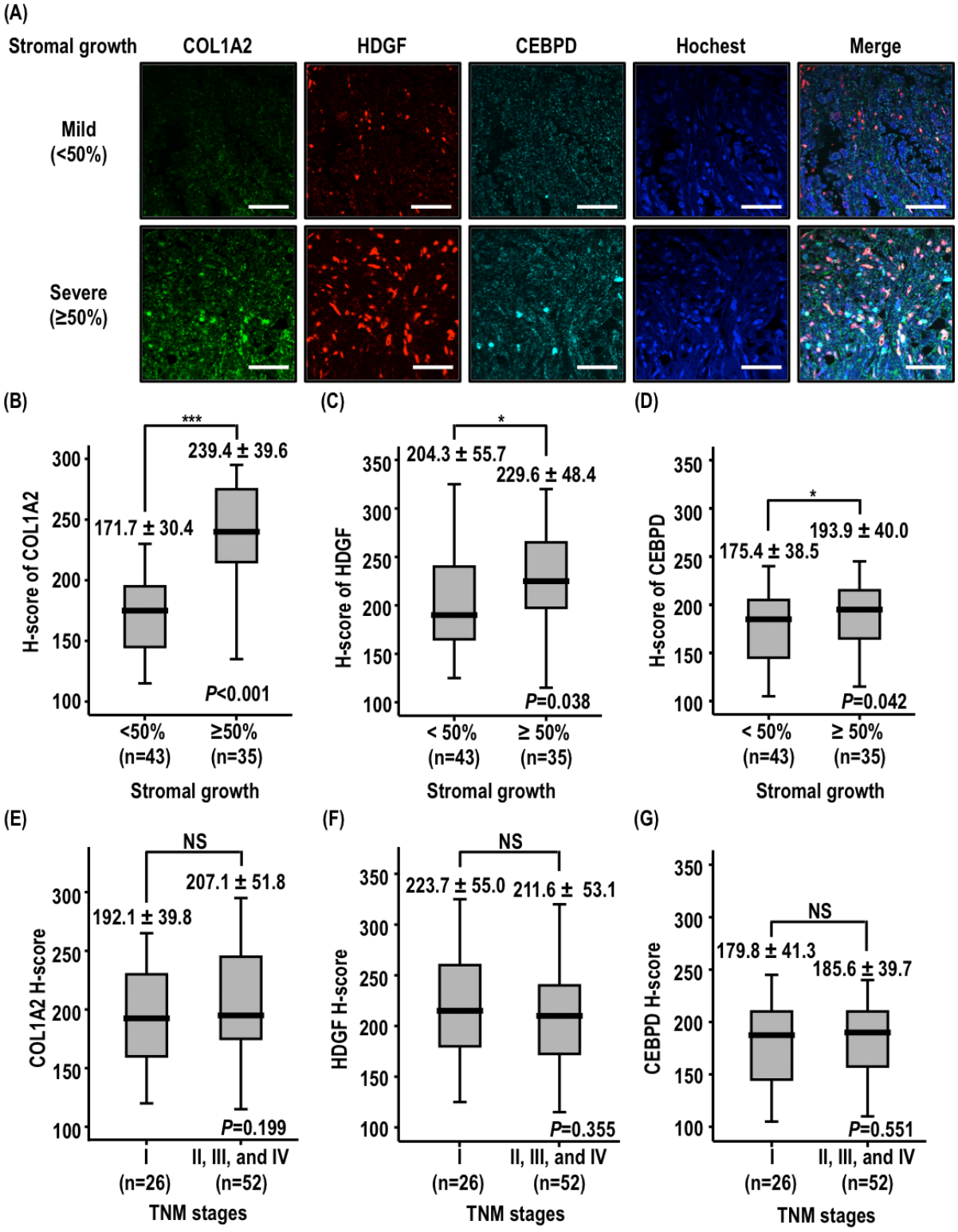
(A)
Stromal growth
COL1A2
HDGF
CEBPD
Hochest
Merge
Mild (<50%)
Severe (≥50%)
(B)
***
239.4 ± 39.6
171.7 ± 30.4
H-score of COL1A2
P<0.001
<50% (n=43)
≥50% (n=35)
Stromal growth
(C)
*
204.3 ± 55.7
229.6 ± 48.4
H-score of HDGF
P=0.038
< 50% (n=43)
≥ 50% (n=35)
Stromal growth
(D)
*
193.9 ± 40.0
175.4 ± 38.5
H-score of CEBPD
P=0.042
< 50% (n=43)
≥ 50% (n=35)
Stromal growth
(E)
NS
207.1 ± 51.8
192.1 ± 39.8
COL1A2 H-score
P=0.199
I (n=26)
II, III, and IV (n=52)
TNM stages
(F)
NS
223.7 ± 55.0
211.6 ± 53.1
HDGF H-score
P=0.355
I (n=26)
II, III, and IV (n=52)
TNM stages
(G)
NS
179.8 ± 41.3
185.6 ± 39.7
CEBPD H-score
P=0.551
I (n=26)
II, III, and IV (n=52)
TNM stages

Figure 6

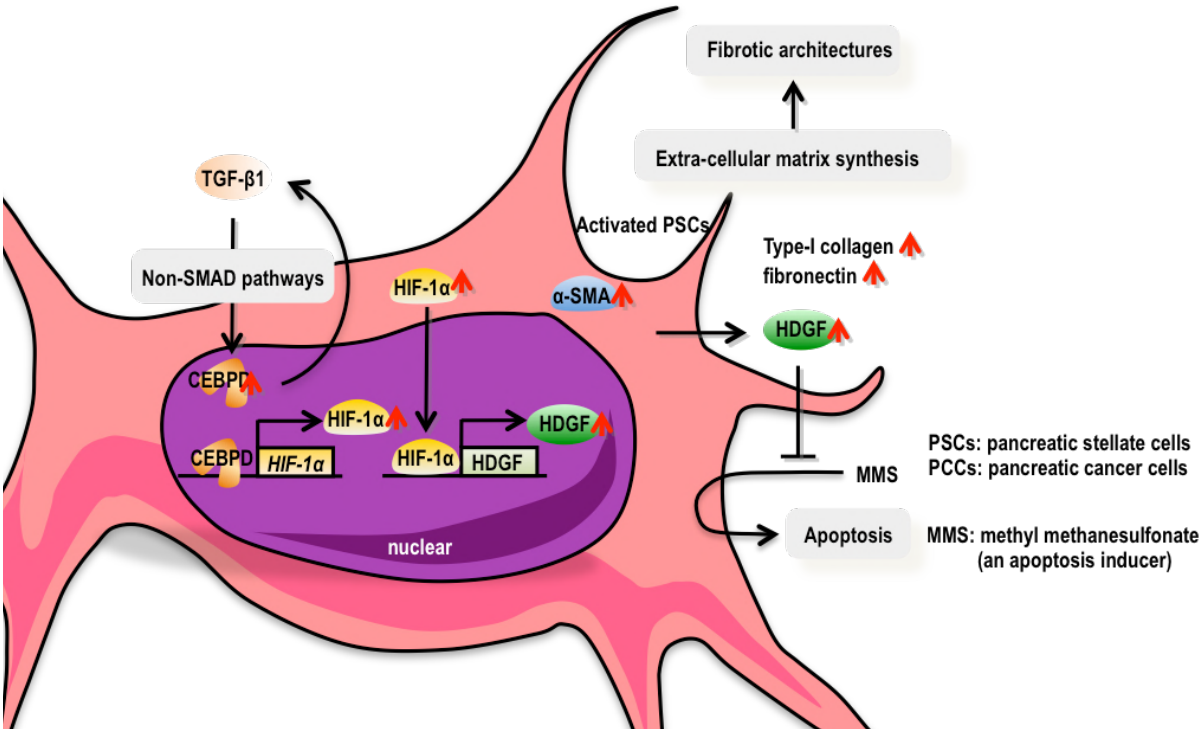
Fibrotic architectures
Extra-cellular matrix synthesis
TGF-β1
Activated PSCs
Type-I collagen
fibronectin
Non-SMAD pathways
HIF-1α
α-SMA
HDGF
CEBPD
HIF-1α
HDGF
CEBPD
HIF-1α
HIF-1α
HDGF
nuclear
MMS
Apoptosis
PSCs: pancreatic stellate cells
PCCs: pancreatic cancer cells
MMS: methyl methanesulfonate
(an apoptosis inducer)